Journal of Computational and Applied Mathematics 234 (2010) 1930–1936

Contents lists available at ScienceDirect

Journal of Computational and Applied Mathematics

journal homepage: www.elsevier.com/locate/cam

# Dispersion of elastic waves in the contact–impact problem of a long cylinder

D. Gabriel, J. Plešek*, R. Kolman, F. Valeš

*Institute of Thermomechanics, Academy of Sciences of the Czech Republic, Dolejškova 5, 182 00 Praha 8, Czech Republic*

ARTICLE INFO

*Article history:*
Received 14 December 2007
Received in revised form 20 June 2008

*Keywords:*
Wave propagation
Dispersion analysis
Serendipity elements
Two cylinder impact

ABSTRACT

Numerical dispersion of two-dimensional finite elements was studied. The outcome of the dispersion study was verified by the numerical and analytical solutions to the longitudinal impact of two long cylindrical bars. In accordance with the results of the dispersion analysis it was demonstrated that the quadratic elements showed better accuracy than the linear ones.



## 1. Introduction

The finite element method simulations of stress waves arising due to contact–impact boundary conditions must cope with the presence of high-frequency components in the loading spectrum. As a consequence severe dispersion of propagating waves is induced on the numerical solution. Despite many papers published on the subject, little attention has been paid so far to higher-order elements. Belytschko and Mullen [1] were the first to extend the dispersion analysis to quadratic one-dimensional finite elements. It was shown that a spurious optical branch in the spectrum existed. The existence of this branch caused the presence of noise associated with the propagation of discontinuities. Later, the dispersion study of the three-dimensional second-order Helmholtz equation was carried out in [2]. The analysis was conducted for trilinear rectangular eight-node elements, for triquadratic rectangular twenty-seven-node elements and for the serendipity rectangular twenty-node elements using various mass approximations. In Refs. [3–5] the recent results accomplished by the authors are summarized, in particular the extension of dispersion analysis to the eight-node serendipity finite elements. Based on the comparison of dispersion curves it was argued that the quadratic finite elements exhibited significantly smaller dispersion than the linear ones.

In this work, the outcome of the theoretical study [3–5] was verified by the finite element and analytical solutions to the longitudinal impact of two long elastic cylinders. The analytical solution of this symmetric contact–impact problem derived in [6] is quite complicated, expressing the distribution of displacements and stresses in the form of infinite series of improper integrals. The model problem was treated as an axisymmetric one, each cylinder discretized by four-node linear elements and eight-node serendipity elements, respectively.

In Section 2 the governing equations of linear elastodynamics are summarized including wave solutions. In Section 3 the proposed numerical–analytical approach for the investigation of dispersion behaviour of higher-order elements, which is fully documented in Ref. [5], is outlined. Furthermore, the dispersion diagrams of the bilinear and serendipity plane elements are presented. The formulas for the element size and limit excitation frequency controlled by the dispersion error are derived in Section 4. Finally, the results of the problem of impact of two elastic cylinders are discussed in Section 5.

* Corresponding author.
*E-mail addresses:* gabriel@it.cas.cz (D. Gabriel), plesek@it.cas.cz (J. Plešek), kolman@it.cas.cz (R. Kolman), vales@cdm.it.cas.cz (F. Valeš).

0377-0427/$ – see front matter 
doi:10.1016/j.cam.2009.08.043

## 2. Plane elastic waves

The equation of motion pertinent to linear elastodynamics can be written in the index notation

$$(\Lambda + G)u_{j,ji} + Gu_{i,jj} = \rho\ddot{u}_i \tag{1}$$

where $\Lambda$ and $G$ are Lamé's constants, $\rho$ is the mass density, $u_i$ and $\ddot{u}_i$ is the $i$th component of the displacement and the acceleration vector, respectively. The Lamé constants $\Lambda$, $G$ may be related to engineering constants $E$, $\nu$ as

$$\Lambda = \frac{\nu E}{(1+\nu)(1-2\nu)}, \qquad G = \frac{E}{2(1+\nu)} \tag{2}$$

where $E$ and $\nu$ are Young's modulus and Poisson's ratio.

In an unbounded isotropic continuum, two types of planar waves exist: the longitudinal wave and two transversal waves, featuring mutually orthogonal polarisation. The longitudinal wave propagates with the speed

$$c_l = \sqrt{\frac{\Lambda + 2G}{\rho}}. \tag{3}$$

The speed of the two transversal waves is

$$c_t = \sqrt{\frac{G}{\rho}}. \tag{4}$$

The standard continuum is said to be *non-dispersive*. This is, by d'Alembert's solution, because the wave profile (wavelength) does not affect the velocity of propagation.

As a special case, one may consider a plane harmonic solution to Eq. (1) as

$$u_i = U_i(\mathbf{x}) \exp(\mathrm{i}k(\mathbf{p}\cdot\mathbf{x} \pm ct)) \tag{5}$$

or in its equivalent form

$$u_i = U_i(\mathbf{x}) \exp(\mathrm{i}(\mathbf{k}\cdot\mathbf{x} \pm \omega t)) \tag{6}$$

where $\mathrm{i} = \sqrt{-1}$ is the imaginary unit; $\mathbf{x}$ is the position vector; $t$ is time; $k$ is the wave number; $\mathbf{p}$ is the unit normal to the wave front; $\mathbf{k}$ is the wave vector, $\mathbf{k} = k\mathbf{p}$; $c$ is the phase velocity; $\omega$ is the angular velocity; and $U_i$ is the $i$th component of the amplitude vector at the point defined by the position vector $\mathbf{x}$. For a given wavelength $\lambda$, the wave number $k$ may be computed from

$$k = \frac{2\pi}{\lambda}. \tag{7}$$

The phase velocity $c$ is related to $\omega$ and $k$ by

$$c = \frac{\omega}{k}. \tag{8}$$

Finally, the group velocity $c_g$ is defined as

$$c_g = \frac{\mathrm{d}\omega}{\mathrm{d}k}. \tag{9}$$

In non-dispersive systems, $c$ is a constant and since $\omega = ck$, we get $c_g = c$. Thus, in the absence of dispersion the group velocity equals the phase velocity. On the other hand, $c_g \neq c$ indicates dispersion.

## 3. Numerical dispersion analysis

The mesh is assumed regular and uniform so only the characteristic patches containing $2 \times 2$ plane strain elements are considered—see Fig. 1. Furthermore, in the bilinear mesh, all the nodes possess the same sub-matrices in the final assembly and thus only one characteristic set of equations corresponding to, say, node $\{m, n\}$ has to be assembled. Likewise, one corner node $\{m, n\}$ and two mid-side nodes $\{m+1, n\}$ and $\{m, n+1\}$ must be taken into account when dealing with the serendipity mesh.

Suppose that the origin of the coordinate system is located at the node $\{m, n\}$. Thus, for the bilinear mesh,

$$x_{m+r} = rH_x, \qquad y_{n+s} = sH_y, \quad \text{for } r, s = 0, \pm 1 \tag{10}$$

and for the serendipity mesh

$$x_{m+r} = rH_x/2, \qquad y_{n+s} = sH_y/2, \quad \text{for } r, s = 0, \pm 1, \pm 2 \tag{11}$$

where $H_x$ and $H_y$ denote the size of the rectangular element (Fig. 1).

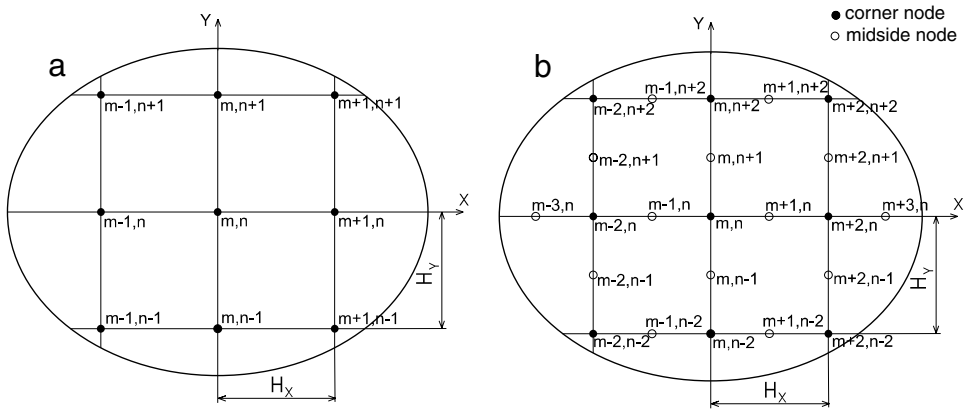


**Fig. 1.** Two-dimensional (a) bilinear (b) serendipity regular finite element mesh.

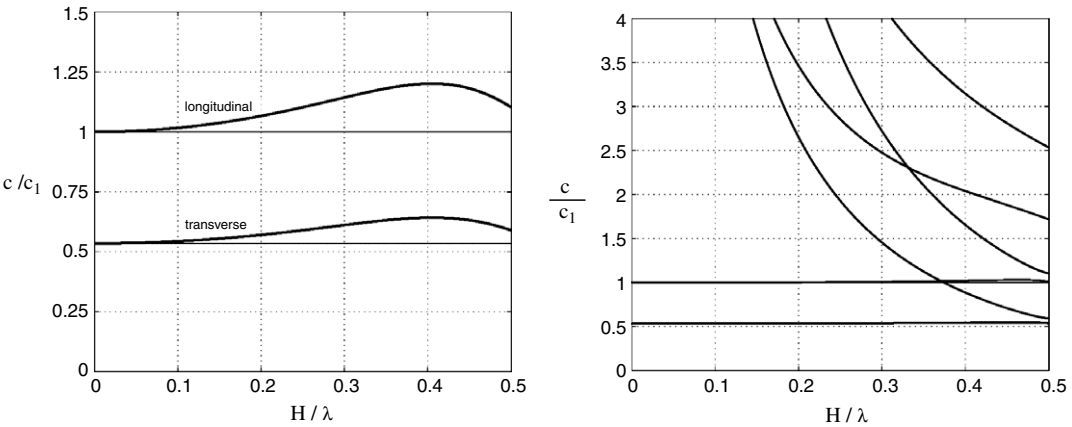


**Fig. 2.** Wave speed versus wave length for bilinear (left) and serendipity (right) elements for angle $\theta = 0°$.

The system of differential equation derived for the nodes of the considered patch can be written as

$$\mathbf{M}_c\ddot{\mathbf{u}}_c + \mathbf{K}_c\mathbf{u}_c = \mathbf{0} \tag{12}$$

where the local consistent mass matrix $\mathbf{M}_c$ and the local stiffness matrix $\mathbf{K}_c$ are of rectangular form $2 \times 18$ and $6 \times 42$ for the bilinear and serendipity elements, respectively.

Next, the classic Fourier analysis follows (see e.g. Refs. [1,7,8]) when the prescribed nodal harmonic solution—a discrete counterpart to Eq. (5)—in the form

$$\begin{aligned} u_{ij} &= U_{ij}\exp\left(\mathrm{i}\frac{2\pi}{\lambda}(p_x x_i + p_y y_j - ct)\right) \\ v_{ij} &= V_{ij}\exp\left(\mathrm{i}\frac{2\pi}{\lambda}(p_x x_i + p_y y_j - ct)\right) \end{aligned} \tag{13}$$

is substituted to the differential equilibrium equations (12). In Eq. (13), $U_{ij}$, $V_{ij}$ are yet unknown amplitudes defining the shape of the deformation mode. The components of the unit normal to the wave front $\mathbf{p}$ may be expressed as

$$p_x = \cos\theta, \qquad p_y = \sin\theta \tag{14}$$

where $\theta$ is the direction of the plane wave propagation through the finite element grid. Although the matrices $\mathbf{M}_c$ and $\mathbf{K}_c$ are non-square, the subsequent use of the difference relations (10), (11) leads to appropriate column compression [7], which gives rise to a symmetric generalized eigenvalue problem (with square matrices). Solving for the eigenvalues the desired dispersion relationship $c = f(\lambda, \theta)$ is obtained.

Comparison of dispersion properties for bilinear and serendipity elements is shown in Fig. 2, where the normalized wave speed $c/c_l$ versus the normalized wave length $H/\lambda$ is drawn for the worst case in terms of dispersion $\theta = 0$. Fig. 2 clearly shows the advantage of quadratic elements over linear ones. There is virtually no dispersion up to the resolution limit $H/\lambda = 0.5$ for quadratic elements.

**Table 1**
Values of $C$ for two element types.

| Admissible relative error of Phase velocity (%) | Linear element | Quadratic element |
|---|---|---|
| 1 | 0.075 | 0.350 |
| 2 | 0.110 | 0.370 |
| 5 | 0.175 | 0.385 |

Furthermore, there are four additional spurious solutions, called the optical modes. They do not really exist in a perfect continuum and should be solely attributed to FE discretization. Discussion of $\omega$–$k$ diagrams carried out in [5] elucidates that these fictitious modes are excited only at very high-frequency loadings, well beyond elements resolution limit, hence they do not really interfere with the acoustic modes. This is indirectly confirmed by the example in Section 5 where the overall accuracy of numerical solutions demonstrates supremacy of the serendipity elements over bilinear ones.

## 4. Choice of element size and time step

Numerical dispersion of the finite element method can be partially eliminated by a suitable choice of the parameters of a numerical model such as the element type, mesh size, integration time step, etc. The influence of time integration schemes, the central difference method and the Newmark method, was studied in [9]. It was proved that the dispersion behaviour strongly depended on the choice of the integration step. However, the effect of time integration diminished when the time step $\Delta t$ defined by the dimensionless Courant number Co did not exceeded

$$\mathrm{Co} = \frac{c_l \Delta t}{H} < 0.5. \tag{15}$$

In Ref. [4] the empirical estimate was derived for the element size

$$H/\lambda < C \tag{16}$$

where the constant $C$ was chosen according to the element type and the admissible relative error of the phase velocity as shown in Table 1. It follows from Table 1 that the relative error of the phase velocity is less than 2% in case the element size is limited by $H < \lambda/3$, i.e. $C \doteq 0.33$ for quadratic mesh and $H < \lambda/10$, i.e. $C \doteq 0.1$ for linear mesh, respectively.

Wavelength $\lambda$ can be estimated from the maximum excitation frequency $\omega_{\max}$, which is bounded by the admissible dispersion error. Then the relation (16) may be arranged with the aid of (7) and (8) to obtain an estimate on the element size

$$H < C \frac{2\pi c_t}{\omega_{\max}} \tag{17}$$

so that the limit imposed on the maximum excitation frequency $\omega_{\max}$ at fixed $H$ reads

$$\omega_{\max} < C \frac{2\pi c_t}{H}. \tag{18}$$

Note that the fulfilment of conditions (17) and (18) is required for the transversal wave speed $c_t$ so that the error bound property will pass on to longitudinal wave propagation as $c_t < c_l$.

## 5. Impact of two long elastic cylinders

The longitudinal impact of two elastic cylinders was studied, for which the analytical solution was available [6]. Simultaneously, symmetric properties of the contact algorithm based on the pre-discretization penalty method [10] were tested.

The cylinders dimensions were: radius $a = 2.5$ mm, length 6.25 mm. Young's modulus, Poisson's ratio and density, respectively, were $E = 2.1 \times 10^5$ MPa, $\nu = 0.3$, $\rho = 7800$ kg/m$^3$. The cylinders made contact with initial velocity $v_0 = 1$ m/s prescribed at time $t = 0$ s. The computation end time, $t = 2a/c_l$, was chosen such that it was less than the time needed for the fastest wave to travel back and forth so that the solution was influenced by no reflected waves. Effectively, the cylinders might be considered infinitely long.

The analytical solution [6] utilizing the Laplace transform is rather complex. The distributions of displacements and stresses are cast in the form of infinite series of improper integrals which are evaluated numerically. For illustration, theoretical positions of wave fronts for time $c_l t/a = 2$ are plotted in Fig. 3. In this figure, $r$, $z$ denote cylindrical coordinates, $a$ the radius of the cylinder and $t$ time, respectively; velocities are renamed as $c_1 = c_l$ and $c_2 = c_t$.

The primary wave front propagates with the speed of longitudinal waves $c_l$. Furthermore, the wave fronts of longitudinal and transversal waves generated by the reflection from boundaries can be observed. The unloading (rarefaction) wave fronts of shear waves propagate with the speed $c_t$. The hatched part corresponds to the state of stress encountered in the impact of two half-spaces.

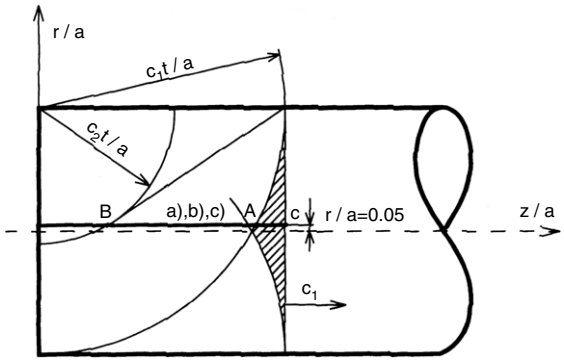


**Fig. 3.** Theoretical position of wave fronts for $c_1 t/a = 2$ after [6].

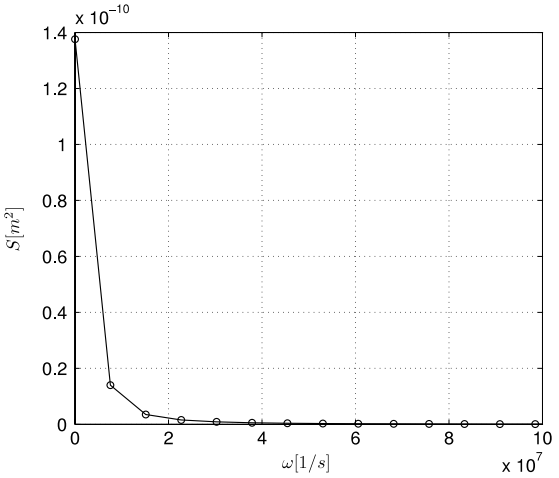


**Fig. 4.** Power spectrum of the cylinder's excitation.

The problem was treated as an axisymmetric one, each cylinder discretized by $100 \times 250$ four-node linear elements and $50 \times 125$ eight-node serendipity elements. The linear mesh was obtained by regular refinement bisecting the quadratic elements at the mid-side nodes. Thus, the total number of degrees of freedom NDOF is greater for the linear mesh (NDOF = 50 702) than for the quadratic one (NDOF = 38 202). The Newmark integration scheme with the consistent mass matrix was employed. In order to suppress the influence of numerical integration, the time step was chosen very small. It was set to $\Delta t = 1.038174 \times 10^{-9}$ s, which corresponds to dimensionless Courant's number Co = 0.25 for linear elements and 0.125 for quadratic elements.

In Section 4 estimates of the element size and the maximum excitation frequency with dispersion error control were derived. In the case when the time distribution of loading is known, it may be expanded as a Fourier series and expressed in terms of its harmonic components. In other words, the frequency spectrum of loading can be determined. In this example, the loading is realized by the contact boundary condition so that no explicit loading is prescribed. However, it is possible to formulate the same problem from another view point: a flying cylinder is moving with initial velocity $v_0$ when it hits the opposite face. At this point, it is sufficient to prescribe its face displacement as $u = -v_0 t$. Thus, disregarding sign, kinematic excitation of the cylinder is defined by a time sampled function

$$u(t_n) = v_0 n \Delta t \tag{19}$$

where $t_n = n\Delta t$ is the time corresponding to the $n$-th time sample. Using the fast Fourier transform, we obtain the power spectrum of the cylinder's excitation $S$ plotted in Fig. 4. It is sufficient to take into account the first 10 terms of this spectrum for the approximation of the function (19). It corresponds to the maximum excitation frequency $\omega_{\max} = 6.817 \times 10^7$ [1/s]. According to expression (18) the admissible maximum frequency $\omega_{\max}^{\text{admissible}} = 8.09 \times 10^7$ [1/s] for the linear mesh and $\omega_{\max}^{\text{admissible}} = 13.48 \times 10^7$ [1/s] for the serendipity mesh might be calculated. In both cases condition (18) was satisfied. Note, that the relations (17) and (18) hold only for a short time after the impact has occurred when the pressure loading caused by the primary longitudinal wave still dominates the stress field and is not significantly influenced by reflections from the cylinder's boundaries.

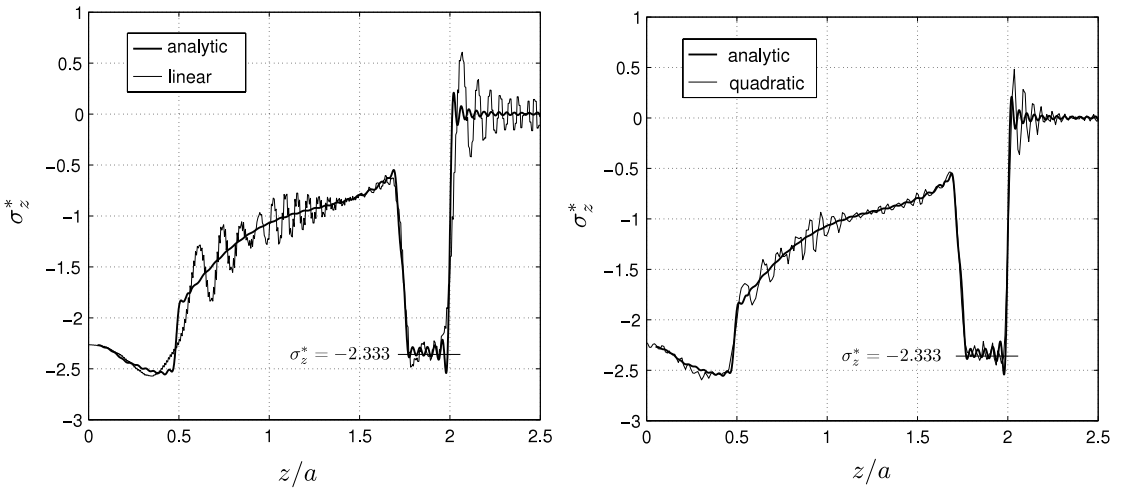


**Fig. 5.** Axial stress distribution along axial coordinate for $c_l t/a = 2$ and $r/a = 0.05$: bilinear (left) and serendipity (right) elements.

Comparison of accuracy for both discretization patterns follows from Fig. 5, where the normalized axial stress distribution $\sigma_z^* = \sigma_z c_l/\lambda v_0$ along the cylinder axis $z/a$ is drawn. The results are plotted for time $c_l t/a = 2$ at a short distance from the axis $r/a = 0.05$ (see Fig. 3). In addition, the analytical solution is plotted in Fig. 5 by the bold line.

It is interesting to note the way the response is influenced by wave fronts of unloading waves (points A and B in Fig. 3). In the region between points A and C the value of axial stress should be identical to the constant value $\sigma_z^* = -2.333$ corresponding to a half-space impact problem. At point C the stress should undergo a step drop from $\sigma_z^* = -2.333$ to zero. It should be pointed out that the accuracy of analytical solution is strongly influenced by the number of terms included in the series of improper integrals [6]. The analytical solution plotted in this paper was derived from the summation of the first 150 terms of this series. However, the value of axial stress significantly oscillates in the region of the "should have been" constant stress. This effect will reduce provided a greater number of terms have been used.

It is obvious that the quadratic elements exhibit better accuracy than the linear ones using even less number of degrees of freedom. In addition, the linear solution shows more "ragged" distribution. This is especially apparent behind the primary wave front corresponding to the state of zero stress. In this pre-front zone, the decay of undesired oscillation is slower than for the quadratic mesh. This example nicely demonstrates capabilities of the two element types and evokes similar conclusions as those drawn from the dispersion distributions compared in Fig. 2.

## 6. Conclusions

Numerical dispersion properties of two-dimensional finite elements in elastodynamics were investigated. We followed a theoretical study [3–5], where the dispersion behaviour of the quadratic eight-node elements with the serendipity type shape functions was analysed. We focused on the verification of this dispersion study by means of comparison of the numerical and analytical solutions to the longitudinal impact of two infinitely long cylindrical bars.

The numerical analysis was treated as an axisymmetric one, each cylinder discretized by four-node linear elements and eight-node serendipity elements, respectively. The Newmark integration scheme with the consistent mass matrix was employed. In order to check out the influence of numerical integration, the time step was chosen very small. For comparison, the analytical solution of this problem expressed in the form of an infinite series of improper integrals was recalled. Excellent agreement between the analytical and finite element solutions utilizing quadratic elements was observed. In accord with the claims of paper [5] it was demonstrated that the quadratic elements showed much better accuracy than linear elements using even less number of degrees of freedom.

Most of the present discussion carries over to three-dimensional problems. This is chiefly due to the fact that the dispersion error reaches its maximum for $\theta = 0$ when a wave propagates parallel to the finite element mesh. If desired, full three-dimensional dispersion analysis may be accomplished in the same fashion.

## Acknowledgements

This work was supported by the Grant Agency of the Czech Republic under grant numbers GA101/07/1471, GA101/09/1630 and GA101/06/0213 in the framework of AV0Z 20760514.

## References

[1] T. Belytschko, R. Mullen, On dispersive properties of finite element solutions, in: Modern Problems in Elastic Wave Propagation, Wiley, New York, 1978, pp. 67–82.
[2] N.N. Abboud, P.M. Pinsky, Finite element dispersion analysis for the three-dimensional second-order scalar wave equation, International Journal for Numerical Methods in Engineering 35 (1992) 1183–1218.

[3] J. Plešek, R. Kolman, M. Okrouhlík, Numerical dispersion of quadratic finite element meshes, in: WCCM VII, University of California, Los Angeles, 16–22 July 2006, CDROM.
[4] J. Plešek, R. Kolman, M. Okrouhlík, On the occurrence of spurious optical modes in transient finite element analysis, in: Mechanics & Materials in Design, University of Porto, Porto, Portugal, 24–26 July 2006, pp. 189–190.
[5] J. Plešek, R. Kolman, D. Gabriel, F. Valeš, Application of dispersion analysis to the finite element solution of wave propagation and impact problems, in: M. Papadrakakis et al. (Eds.), COMPDYN 2007, ECCOMAS 2007, pp. 1–12.
[6] F. Valeš, Š. Morávka, R. Brepta, J. Červ, Wave propagation in a thick cylindrical bar due to longitudinal impact, JSME International Journal, Series A 39 (1) (1996) 60–70.
[7] R. Mullen, T. Belytschko, Dispersion analysis of finite element semi-discretizations of the two-dimensional wave equation, International Journal for Numerical Methods in Engineering 18 (1982) 11–29.
[8] L.L. Thompson, P.M. Pinsky, A Galerkin least squares finite element method for the two-dimensional Helmholtz equation, International Journal for Numerical Methods in Engineering 28 (1995) 371–397.
[9] R. Kolman, M. Okrouhlík, J. Plešek, The effect of time integration on the dispersion properties of quadratic finite elements in elasto-dynamics, in: J. Vimmr (Ed.), Computational Mechanics 2005, University of West Bohemia in Pilsen, Pilsen, 7–9 November 2005, pp. 315–322.
[10] D. Gabriel, J. Plešek, M. Ulbin, Symmetry preserving algorithm for large displacement frictionless contact by the pre-discretization penalty method, International Journal for Numerical Methods in Engineering 61 (2004) 2615–2638.